Ultrafast optical beam deflection in a pump probe configuration*

Lingliang Liang(梁玲亮)[1,2,3,†], Jinshou Tian (田进寿)[1], Tao Wang(汪 韬)[1], Shengli Wu(吴胜利)[3], Fuli Li(李福利)[3], Junfeng Wang(王俊锋)[1], and Guilong Gao(高贵龙)[1,2,3]

[1] *State Key Laboratory of Transient Optics and Photonics, Xi'an Institute of Optics and Precision Mechanics of Chinese Academy of Sciences, Xi'an* 710119, *China*

[2] *University of Chinese Academy of Sciences, Beijing* 100049, *China*

[3] *Xi'an Jiaotong University, Xi'an* 710049, *China*

(Received 26 January 2016; revised manuscript received 11 June 2016; published online 20 July 2016)

Propagation of a signal beam in an AlGaAs/GaAs waveguide multiple-prism light deflector is theoretically investigated by solving the scalar Helmholtz equation to obtain the dependences of the temporal and spatial resolvable characteristics of the ultrafast deflector on the material dispersion of GaAs including group velocity dispersion and angular dispersion, interface reflection, and interface scattering of multiple-prism deflector. Furthermore, we experimentally confirm that, in this ultrafast beam deflection device, the deflecting angle of the signal light beam is linear with the pump fluence and the temporal resolution of the ultrafast deflection is 10 ps. Our results show that the improvement of the temporal and spatial resolvable performances is possible by properly choosing the structural parameters and enhancing the quality of the device.

Keywords: pump probe, ultrafast deflection, multiple-prism light deflector, temporal resolution

PACS: 06.60.Jn, 07.60.–j, 42.25.Bs, 42.79.Fm **DOI:** 10.1088/1674-1056/25/9/090602

1. Introduction

Optical beam deflecting and scanning have found many applications in civil and military systems. The available techniques include mechanical, acousto–optic, electro–optic, all-optical devices and so on.[1–4] Among them, the mechanical deflectors are limited in developing owing to their low deflecting speed. The acousto–optic devices had been most interesting, but their access speed and resolvable power are still not high enough. Although electro–optic deflectors can scan faster comparatively, the relative phase change induced by electro–optic effect is small in most of the electro–optic materials. Thus it requires a long optical path length in these electro–optic crystals, which is limited by the materials themselves.[5] In addition, the driving power for the electro–optic devices is mostly large. The polymeric material has been reported to be a promising candidate instead of the electro–optic crystal, because of its compatibility with different substrates, ease of fabrication, low cost, and not so high driving voltage as the electro–optic material, despite a lack of thermal stability and relatively large insertion losses.[6] Borrowing the method in phased array radar, many phased array optical scanning devices have been implemented.[7,8] However, none of these approaches are ultrafast enough to apply in the ultrafast light signal scanning/steering. The present popular ultrafast travelling-wave electro–optic deflector employs a quasi-velocity-matching technique to compensate the velocity mis-match between an optical group velocity and a microwave phase velocity, which can operate in a picosecond timescale.[9] Furthermore, light deflecting controlled with light is also proposed,[10–12] some of which can easily promote an ultrafast light deflection.

The development of the ultrafast optical deflecting/scanning devices brings an inspiration for the improvement of many optical and photoelectric devices. Take the image converting tube streak camera as an example. The meander-type travelling-wave deflecting plate takes the place of the more conventional standing-wave parallel-plate to acquire both increased deflection sensitivity and frequency bandwidth.[13,14] To proceed, the fact that space charge effect leads to a trade-off between the temporal resolution and dynamic range when the signal energy is high is becoming a serious obstacle for the further performance improvement of this image converting tube streak camera.[15] In the early stages, direct deflecting of the optical beam using an electro–optic deflector had been proposed instead of photoelectron beam scanning manner in the image converting tube streak camera.[16] In the year of 2010, Chris's group first demonstrated that the serrated light illumination for deflection-encoded recording (SLIDER) concept enables the single shot all-optical solid state camera, which is an example of direct beam scanning.[17] There are plenty of other applications that can benefit from the development of the optical deflecting devices.[18–20]

In our previous work, we have investigated the statically deflecting characteristics of a CW signal laser at the wavelength of 1053 nm passing through a multiple-prism deflector under the illumination by a 800 nm CW pump laser.[21]

*Project supported by the National Natural Science Foundation of China (Grant Nos. 11274377 and 61176006) and the State Major Research Equipment Project, China (Grant No. ZDY2011-2).

†Corresponding author. E-mail: lianglingliang@opt.cn

© 2016 Chinese Physical Society and IOP Publishing Ltd

This work will research an ultrafast beam deflection by arranging the same multiple-prism deflector in the pump probe configuration. Pump probe technique has been successfully and universally applied to investigate the carrier dynamics of the photo-excited materials, where two ultrafast pulses with arbitrary time delay complete the scanning of the dynamic process. By adjusting the time delay between the pump pulse and the probe pulse (denoted as signal pulse in our context), the deflection of the signal light beam can be linearly controlled. The multiple-prism deflector employs an AlGaAs/GaAs waveguide with a serrated gold mask on its surface to realize the discrete deflection of the signal light beam. Study on the transient absorption or transmission of the intrinsic GaAs has shown that the generation of the non-equilibrium free carriers can be recognized as instantaneous as the pulse duration time and their relaxation time can come up to nanosecond scale.[22,23] Therefore, high response speed and high repetition are allowed in this ultrafast deflection device. In the context, Section 2 gives a theoretical study on the dependences of temporal and spatial resolvable performances on the material dispersion of GaAs including group velocity dispersion and angular dispersion, interface reflection, and interface scattering of the deflector. Section 3 demonstrates the experiments about this ultrafast deflection device. The experimental results show that the temporal resolution is about 10 ps, which is not so much satisfying but really promising in the ultrafast signal scanning, optical communication, light controlling and switching.

2. Theory

2.1. The model

Figure 1 shows the two-dimensional (2D) sketch of the propagation of a light beam in a multiple-prism deflector. The white triangles represent the domains with a photo-induced refractive index change of Δn. According to Bennett's study, the photo-induced refractive index change can reach the order of 0.01–0.1 in GaAs with the effects of bandfilling, bandgap shrinkage, and free carrier absorption.[24] In addition, with the combination of the three effects, the total refractive index change is always negative for the photon energies below the band gap in GaAs. Therefore, as shown in Fig. 1, the light beam is bent towards the negative x direction.

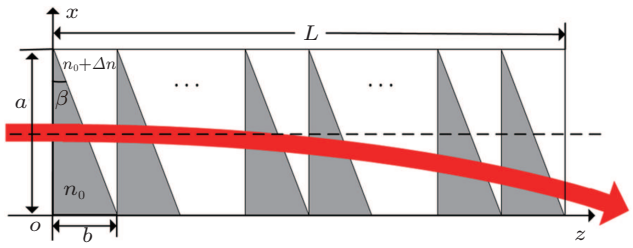


Fig. 1. (color online) Sketch of the propagation of a light beam in a multiple-prism deflector.

The refractive index distribution of a multiple-prism deflector can be expressed as

$$n(x,z,\omega) = n_0(\omega) + \Delta n(x,z), \tag{1}$$

with

$$\Delta n(x,z) = \begin{cases} \Delta n, & x \geq a(1-z/b)+(N-1)b, \\ 0, & \text{else}. \end{cases} \tag{2}$$
$$0 \leq x \leq a,\ 0 \leq z \leq Nb,\ N = 1,2,...,N_t,$$

where ω is the angular frequency of the light beam and N_t is the prism number of the deflector. The electric field of the light beam at any position in the deflector can be obtained by solving the Helmholtz equation. The 2D Helmholtz equation in the frequency domain is expressed as

$$\left[\frac{\partial^2}{\partial x^2} + \frac{\partial^2}{\partial z^2} + k_0^2 n^2(x,z,\omega)\right] E(x,z,\omega) = 0, \tag{3}$$

where k_0 is free space wave number and $E(x, z, \omega)$ represents the scalar field of the light in the deflector.

If the incident light beam is a temporal ultrafast signal, we can resort to Fourier analysis. $E_0(x, z, t)$ is the initial electric field of the ultrafast signal. The Fourier transform of the initial electric field is

$$E_0(x,z,\omega) = \frac{1}{2\pi}\int_{-\infty}^{\infty} E_0(x,z,t)\exp(-\mathrm{j}\omega t)\mathrm{d}t. \tag{4}$$

Denoting $E_t(x, z, \omega)$ as the output field in frequency domain, we can obtain the temporal output field through inverse Fourier transform

$$E_t(x,z,t) = \int_{-\infty}^{\infty} E_t(x,z,\omega)\exp(\mathrm{j}\omega t)\mathrm{d}\omega. \tag{5}$$

The output light intensity can be given by

$$I_t(x,z,t) = |E_t(x,z,t)|^2. \tag{6}$$

2.2. Calculation and Simulation

The temporal resolution of the ultrafast deflector can be simply defined as $t_r = T/M$. T is the time that the light signal spends passing through the entire length of the deflector and $T = L/v_s$. L is the entire length of the deflector and v_s is the group velocity of the ultrafast signal light in the deflector. The number of the resolvable spots of the deflector is obtained by $M = \theta/\delta\theta$, where θ is the deflecting angle and $\theta = L\Delta n/a$, $\delta\theta$ is the angular resolvability of Gaussian beam and $\delta\theta = \sqrt{2\ln 2}\lambda/\pi w_s$. According to the spatial resolution expression, $M \propto \Delta n$ and $M \propto w_s/a$. Particularly by improving the photo-induced refractive index change[25] and increasing the ratio of signal spot width to the width of the prism, the spatial resolution can be greatly improved. It is noted that the spot size of the signal should not exceed half of a as suggested in Ref. [26] for the purpose to obtain a relatively high-quality electric field profile. Based on this premise, it is better to further increase the width of prism to make the waveguide satisfy

the planar waveguide approximation, which is of benefit to the improvement of the spatial resolution. Apart from these, there are several other factors that significantly affect the temporal and spatial resolvable characteristics, which are discussed in the following simulation.

In the simulation, propagation of the light beam in a multiple-prism deflector surrounded by free space is investigated through solving 2D Helmholtz equation by a finite element method with a given initial field profile. The dimensions of the deflector are $a \times N_t b$, where $a = 100$ μm, $b = 13$ μm, and N_t is the total number of prisms. The evaluations of a and b here are the reduced scale of the dimensions of the experimental sample in a proportional ratio of 3:5. The refractive index change Δn is equal to 0.01 (the negative sign is omitted in the context, for it only matters with the deflection direction of the signal beam) according to Bennett's study. Figure 2 displays the deflecting trajectory of the light beam propagating in a multiple-prism deflector, which is obtained by solving Eq. (3). Therefore, the electric field profile of the beam at any position can be extracted from Fig. 2.

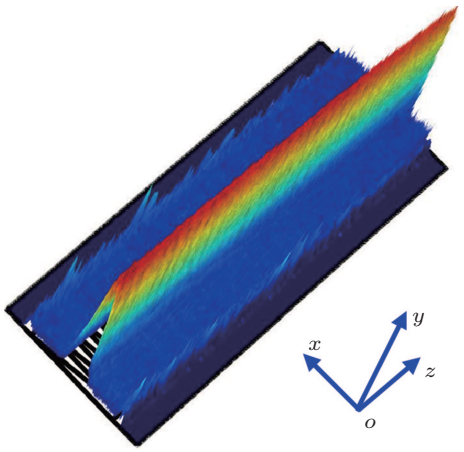


Fig. 2. (color online) Deflection trajectory of the Gaussian signal light beam in a multiple-prism deflector.

2.2.1. Influences of material dispersion and interface reflection on temporal resolution

The initial field of the incident ultrashort pulse is supposed to have a Gaussian expression

$$G_0(x,z,t) = A_0 \exp\left[-\frac{(x-a/2)^2}{w_s^2}\right] \exp\left[\mathrm{j}\omega_0 t - \frac{t^2}{\tau^2}\right], \quad (7)$$

where A_0 is the electric field amplitude, w_s is the cross-section radius of the beam spot, ω_0 is the central angular frequency of the incident pulse, and τ is the temporal 1/e half width. The Fourier transform of $G_0(x, z, t)$ is

$$G_0(x,z,\omega) = A_0 \exp\left[-\frac{(x-a/2)^2}{w_s^2}\right] \times \frac{\tau}{2\sqrt{\pi}} \exp\left[-\frac{\tau^2(\omega-\omega_0)^2}{4}\right]. \quad (8)$$

The intensity of the output pulse from our laser has a nearly Gaussian distribution with a center wavelength of $\lambda_0 =$ 1 μm and a pulse duration (1/e full width) of 120 fs. Therefore, $\tau = 85$ fs. The spectral 1/e half width of the incident temporal pulse is $\Delta\omega/2 = 2/\tau$, accordingly, $\Delta\lambda = 25$ nm (full width).

The material dispersion of GaAs can be given by Sellmeyer formula

$$n_0^2(\lambda) = 8.05 + \frac{2.054}{1 - 0.39/\lambda^2}, \quad (9)$$

where the unit of λ is μm.

Figure 3(a) illustrates the dispersion curve of GaAs based on Eq. (9) as well as the transmissions of light with different wavelength. It can be seen that the energy loss of the light can reach nearly 30% due to interface reflections. Energy loss of the ultrashort pulse always leads to the broadening of the width of the pulse envelope. Figure 3(b) shows the corresponding spectrums of incident ultrashort pulse and output pulse, from which the spectral 1/e full width of output pulse can be calculated to be 20 nm. Then the temporal half width of the output electric field can be obtained to be 106 fs. Compared to the initial 85 fs, the full width broadening is nearly 40 fs. Moreover, combining with the influences of absorption effects such as free carrier absorption, the temporal resolution will become even worse.

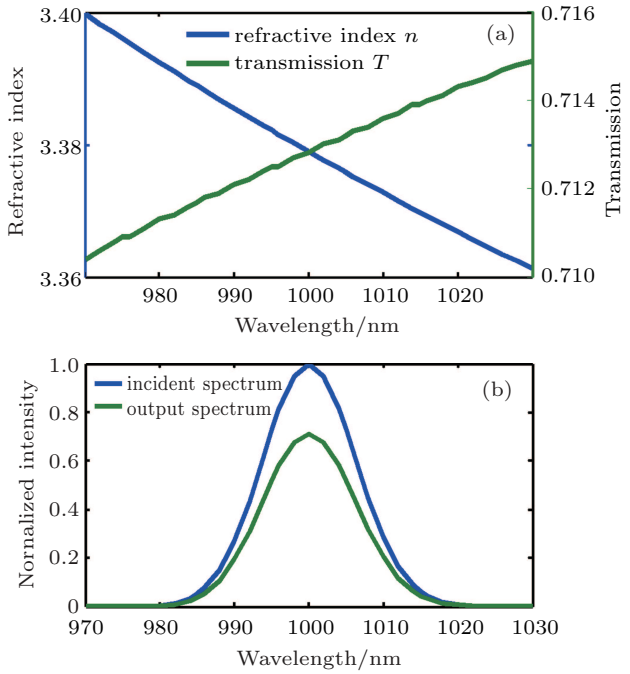


Fig. 3. (color online) (a) The refractive index in GaAs and the transmissions of light with respect to different wavelength. (b) The spectrums of the incident Gaussian pulse and output pulse.

On the other hand, the dependence of material refractive index on the wavelength has two effects on the ultrafast signal pulse propagating in a multiple-prism deflector, one in space termed as angular dispersion (AD) and the other in time

termed as group velocity dispersion (GVD). Both can result in the width broadening of the signal pulse. The GVD brings about the group delay dispersion (GDD), while the AD always yields negative group delay dispersion. The temporal resolution of an ultrafast deflector can also be characterized by the broadened width of an ultrashort pulse passing through the deflector. The broadened full width of signal light field $\Delta\tau$ relating to the GDD can be expressed as $\Delta\tau = \mathrm{GDD}\times\Delta\omega$. The net GDD of the ultrafast signal pulse after propagating the deflector due to AD and GVD can be directly acquired by taking the second derivative of the spectral phase $\varphi(\omega)$ of the deflected signal field with respect to ω, that is

$$\mathrm{GDD} = \left.\frac{\mathrm{d}^2\varphi(\omega)}{\mathrm{d}\omega^2}\right|_{\omega_0} \approx \left[-L\frac{\lambda_0^3}{2\pi c^2}\left(\left.\frac{\mathrm{d}\theta}{\mathrm{d}\lambda}\right|_{\lambda_0}\right)^2\right] + L\frac{\lambda_0^3}{2\pi c^2}\left.\frac{\mathrm{d}^2 n}{\mathrm{d}\lambda^2}\right|_{\lambda_0}, \quad (10)$$

where λ_0 is the central wavelength of the signal light, c is the speed of light in the free space, and L is the entire length of the deflector.[27] The first term of the summation at the right of Eq. (10) is due to AD, and the second term is due to GVD. Figure 4 gives the deflecting angle of signal light beam exiting the end face of the deflector when the wavelength of the incident monochromatic light is changing from 970 nm to 1030 nm. Therefore, the GDD due to AD can be easily estimated. Combining Eqs. (1) and (9), the GDD due to GVD can also be easily obtained. Thus the net broadened width of the signal pulse $\Delta\tau$ is calculated to be ~ 370 fs.

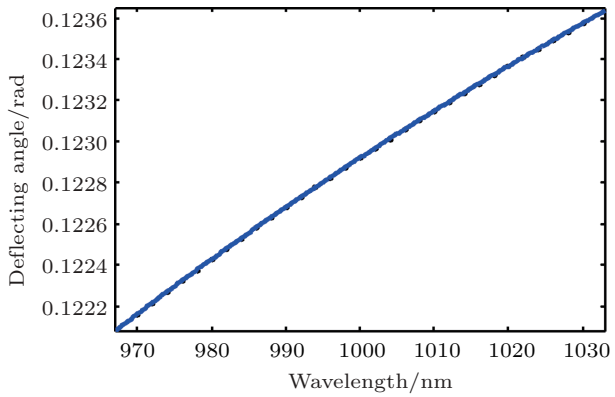


Fig. 4. (color online) The deflecting angle of the signal light beam with respect to different wavelength of signal light.

2.2.2. Influences of interface scattering on spatial resolution

Apart from the effect of material dispersion on the temporal resolution, the structural parameters of the deflector will greatly impact its spatial resolvable and thus the temporal resolvable characteristics. The total deflecting angle of the multiple-prism deflector can be obtained by $\theta = L\Delta n/a$ under the paraxial approximation. It can be seen that the formula to calculate the deflecting angle depends only on the overall dimension of the deflector and is independent of how the deflector is subdivided into individual prisms, on the conditions that the interfaces between adjacent prisms are straight lines and the lines are joined end to end. However, the subdivision style has an impact on the quality of the electric field profile. The electric field profile of the deflection beam at the end face of the deflector is used to investigate the spatial resolvable characteristics of the deflector.

Based on the above analysis, we examine the influences of the structural parameters Δn, N_t, w_s, and different subdivision styles on the profiles of the output electric field. Figure 5(a) shows the electric field norms of the beam at the end face of the deflector when $\Delta n = 0.01$, 0.03, and 0.05. For simplicity, the number of the prisms N_t is assumed to be 20 in the simulation, which is enough for a clarifying description, and the incident beam spot size w_s is 10 μm. It can be seen that from Fig. 5(a), besides different deflection displacements, a slight enlargement of the spot size can be observed in the field profile with larger Δn. No serious distortions are found in these three electric field profiles. Therefore, Δn can be set to be 0.05 in the following simulation for the purpose that an obvious deflection displacement can be observed. Figure 5(b) shows the electric field norms of the beam at the end face of the deflector with different number of prisms. It can be found that with the increasing of N_t, the electric field profile of the beam gradually deteriorates and the beam diameter increases as well, which will ultimately blur the spatial resolution. It seems from Fig. 5(b) that multiple interface refraction will enhance the deterioration of the field profile. However, we cannot easily conclude that increasing number of the interface refractions is responsible for this deterioration. In Fig. 5(c), the electric field norm profiles of two different division styles of deflector with $N_\mathrm{t} = 20$ and 40 are demonstrated under the conditions that the entire length of the deflector is unchanging. The quality of the electric field profile when $N_\mathrm{t} = 40$ is obviously better than that when $N_\mathrm{t} = 20$. The reason is that the incident angles of the light beam at the interfaces are larger when $N_\mathrm{t} = 20$, which will result in a more significant amount of both scattering and reflection at the interfaces and cause the deterioration of the field profiles. This also accounts for the width broadening in Fig. 5(a) with the increase of the refractive index change. The deflection electric field profiles of light beam with different beam spot sizes are also illustrated in Fig. 5(d). According to the expression of angular resolvability of the Gaussian beam, a larger spot size is of benefit to the improvement of the number of the resolvable spots of the deflector. However, from Fig. 5(d), it can be seen that a larger spot size, usually involving a larger interaction range, can still result in the enlargement of the beam spot and the deterioration of the electric field norm profile.

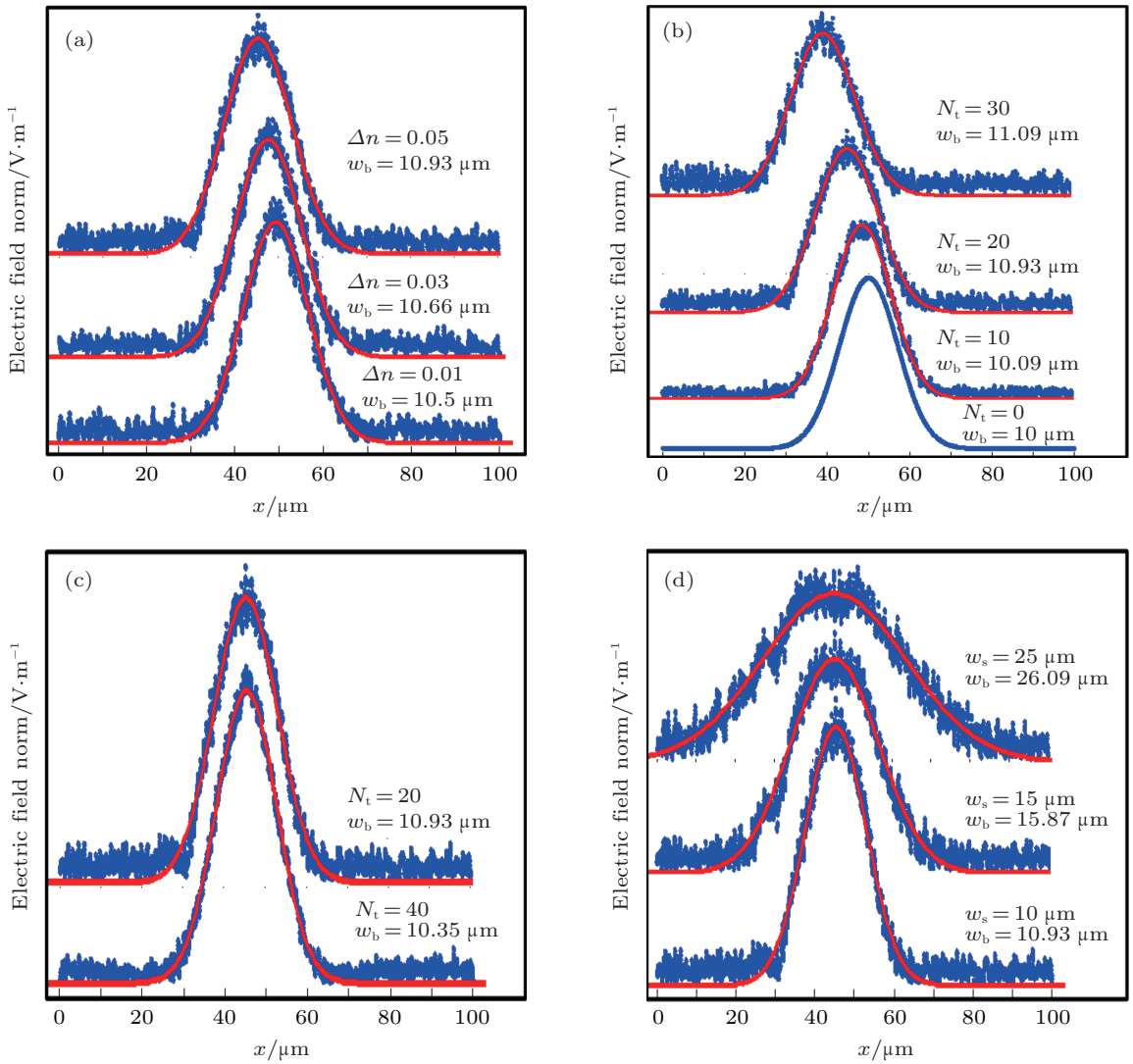


Fig. 5. (color online) The deflection electric field norms of the beam at the end face of the deflector, when (a) $N_t = 20$, $w_s = 10$ μm, $\Delta n = 0.01$, 0.03, and 0.05; (b) $\Delta n = 0.05$, $w_s = 10$ μm, $N_t = 0$, 10, 20, and 30; (c) $\Delta n = 0.05$, $w_s = 10$ μm, $N_t = 20$ and 40 with two different division styles by keeping the total length of the deflector unchanged; (d) $\Delta n = 0.05$, $N_t = 20$, $w_s = 10$ μm, 15 μm, and 25 μm. Here, w_b is the broadening width of field profile obtained by curve fitting.

3. Experiment

The semiconductor material is fabricated by the molecular beam epitaxy (MBE). The undoped waveguide core is a 0.6-μm-thick layer of GaAs, which is sandwiched between a 2-μm-thick upper cladding layer ($Al_{0.24}Ga_{0.76}As$) and 3-μm-thick lower cladding layer ($Al_{0.24}Ga_{0.76}As$) on top of a GaAs substrate. On the waveguide surface, a serrated gold mask is formed by photolithography. The serrated mask is an array of right triangles with two leg lengths of 350 μm and 45 μm, respectively. The number of the triangles N_t is 100. The layering structure of optical deflector is shown in the inset of Fig. 6. The experiments are performed at room temperature.

The experimental setup for ultrafast light deflection is shown in Fig. 6. The delivered ultrashort pulse from the laser has a time duration of 120 fs, a center wavelength of 800 nm and a repetition rate of 1 kHz. The average output power is 3.5 W. The output beam is then split into two portions: one acts as the pump beam with the spot diameter of 8 mm, and the other is coupled into the optical parametric amplifier (OPA TOPAS) to generate a 1000-nm signal beam with a power of 20 mW after being filtered by a triangular prism.

As shown in Fig. 6, the signal beam is coupled into the waveguide core by a cylindrical lens with a focus length of 10 mm. Because of refractive index step at the two side faces of the deflector, the GaAs deflector in fact has a structure of rectangular waveguide in the *xoz* plane. Therefore, there are many mode spots in the *x*-axis direction in the GaAs core. To ensure high spatial resolution, a 25-μm-wide slit is perpendicularly placed just in front of the deflector to choose the mode spot near the origin *o* to investigate, which is not illustrated in Fig. 6. A 25-μm-wide slit in the *x* direction is horizontally placed just after the waveguide to block the light propagating through the substrate and the light glancing incident on and then reflected by the deflector surface, which only

allows the signal propagating through the waveguide core to pass through. A 10× microscope objective is used to image the near-field intensity distribution of signal beam on the end face of the deflector onto a Charge Coupled Device (CCD). Hence the coupling of the signal beam into the waveguide can be checked effectively. The normally incident pump beam is shaped by a cylindrical lens and then illuminates on the upper surface of the deflector. Modulated by the serrated mask, the pump beam instantaneously induces a refractive index change in the GaAs region without the cover of the serrated mask, and thus excites an array of prisms in the waveguide core. The AlGaAs upper cladding layer is transparent to the pump light. The prism array remains latched for a period depending on the relaxation time of photo-injected free carriers in intrinsic GaAs.

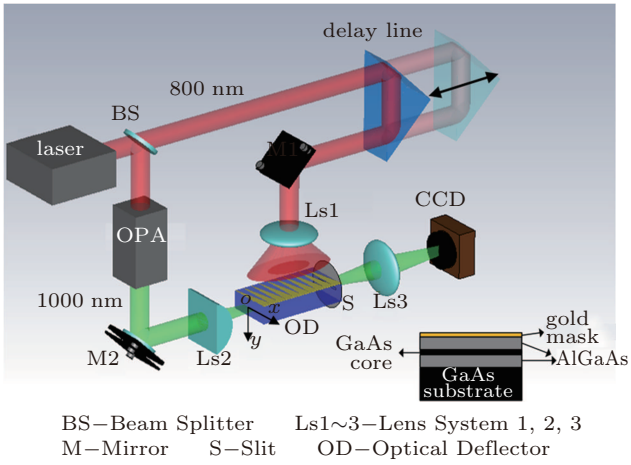


Fig. 6. (color online) The experiment setup for ultrafast light deflection.

At the beginning of the experiment, the pump pulse arrives at the upper surface of the deflector when the signal pulse just begins to exit from its end face. In this case, the signal pulse has no deflection. By gradually decreasing the optical path of the pump pulse, the signal pulse will experience an increasing number of prisms and obtain corresponding deflection. At the moment when the signal pulse propagates through the entire prism array, it will obtain a maximum deflection. Out from the deflector, the deflected signal is focused and coupled onto a CCD camera for recording.

The group refractive index corresponding to the ultrashort signal pulse with a center wavelength of 1000 nm is denoted as n_s. In GaAs, $n_s = 3.8$. Therefore, $T = 57$ ps for the deflector sample. Figure 7 gives the deflecting angle of the signal light beam with the increase of the pump fluence when the delay time of the pump pulse is about 60 ps. The result shows that the deflecting angle of the signal light beam is linear to the pump fluence. High deflection sensitivity is often necessary for a light deflector. Therefore, a pump fluence as high as 320 μJ/cm^2 is applied in the following experiment. Fluence even higher than 320 μJ/cm^2 causes fast deterioration of the streak image of the signal light on the CCD in our experiment. Possible reasons for this include the serious free carrier absorption effect and the limitation of the CCD dynamic range. From Fig. 7, the maximum deflecting angle is 86.4 mrad. Therefore, with $L = 4500$ μm and $a = 350$ μm, the photo-induced refractive index change Δn can be estimated to be ∼0.025 under the pump fluence of 320 μJ/cm^2. According to Ref. [28], the concentration of the free carrier here is estimated to be 2.5×10^{18} cm^{-3} based on the photon energy of pump pulse and band structure of GaAs. Correspondingly, the refractive index change is calculated to be 0.016. The differences may be attributed to the uncertainty of the concentration of the photo-induced free carrier. In addition, there is a great difference between the experiment result of 86.4 mrad and the theoretical calculation in Fig. 4, which needs our further efforts to improve the quality of the deflector sample.

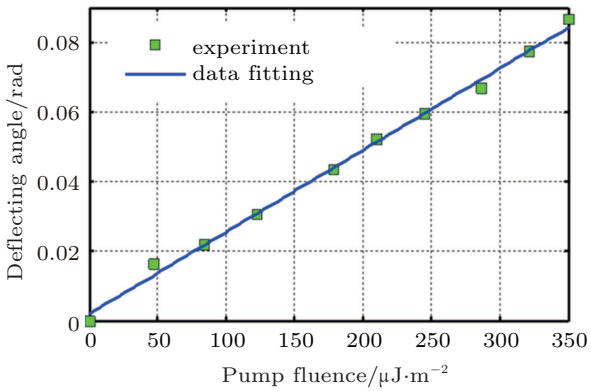


Fig. 7. (color online) Deflecting angle of signal light beam with the increase of the pump fluence.

Figure 8 depicts the deflecting angle of the signal light beam with different delay time of pump pulse. It can be seen that the signal pulse has no deflection when the time delay is less than zero, for the signal pulse has emitted from the waveguide when the pump pulse works. Afterward, the deflecting angle is linearly increasing with the delay time (or propagating distance along z-axis) until a maximum at last.

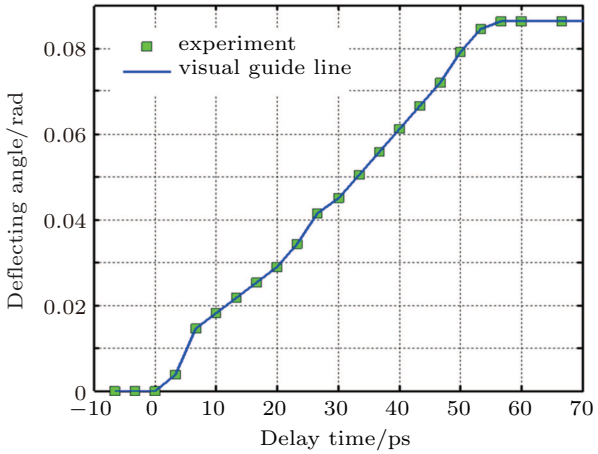


Fig. 8. (color online) Deflecting angles of the signal light beam with different delay time relative to the pump pulse.

As shown in Figs. 7 and 8, the deflection of the signal light beam is proportional to the pump fluence on the deflector, and is also proportional to the delay time between the pump pulse and signal pulse. Therefore, this ultrafast deflector can operate in two ways. First, we can employ the rising edge of a laser pulse, which is on the timescale of T, as the pump illumination to induce a refractive index profile in the deflector, thus realizing the ultrafast deflection of the signal light beam. Second, as mentioned above, make sure that the ultrashort pump pulse arrives at the deflector as soon as the leading part of the ultrafast signal light begins to exit the deflector, and then the time slices of flight across the duration time of ultrafast signal light just represent the delay time between the pump pulse and the corresponding ultrafast signal elements. Therefore, the temporal elements in this ultrafast signal experience an increasing deflection with the time of flight. Both operational styles of the deflector are recognized as instantaneous as the generating time of non-equilibrium free carrier on a timescale of laser pulse duration time.

Figure 9(a) gives the grey levels of the streak images of the signal light beam with different deflections, which are picked up from Fig. 8 with 10-ps time interval. This 10-ps time interval ensures that the streak can be right distinguished from the neighboring one. Therefore, this ultrafast deflection device has a temporal resolution of 10 ps. The flat tops of the curves in Fig. 9(a) result from the limitation of the dynamic range of CCD. It can be seen that the displacement of the sixth curve, representing the streak intensity distribution at $t_{\rm d} = 50$ ps relative to the temporal origin, is 194 μm, which is larger than the half width of the deflector of 175 μm. The reasons for this include the following aspects: (i) the magnification of the focusing lens in the experiment is calculated to be ∼2.2, which is inaccurate; (ii) the center of the incident signal light beam deviates from the width center of the deflector; (iii) the serrated gold mask does not strictly fully cover the upper surface of the bar-type deflector in the sample fabrication process, which directly results in a little larger deflection of the signal light beam than that in the ideal situation; (iv) the synchronization error between the signal light pulse and pump pulse is another possible reason.

Figure 9(b) gives the streak image of the signal light beam corresponding to Fig. 9(a). The width of the streak can be achieved. It also can be seen that the light intensity decreases with the increase of the delay time, which may result from the more serious free carrier absorption when the signal light beam propagates a longer pump-modulated region. Consequently, the streak width of the signal light beam decreases from about 100 μm to 73 μm. Based on the theoretical simulations, angular dispersion and interface scattering contribute to the enlargement of signal beam spot size. In the experiment, we have to raise the signal beam power for the purpose of recognizing the streak image with larger delay time, which exactly results in the over-exposure of the first four streaks at the same power. It is known that the formula about the relationship between deflecting displacement $X(z)$ and the propagating distance z is expressed as $X(z) = \Delta n z^2/(2a)$ for a multiple-prism deflector. It should be noted here that the deflecting displacements seems to be proportional to the delay time or the propagating distances, which is due to the fairly small quadratic coefficient $\Delta n/(2a)$.

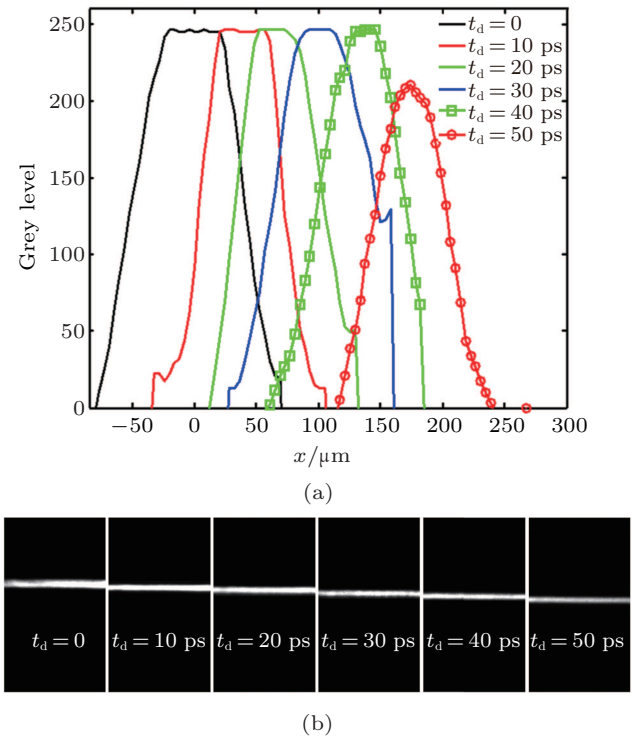


Fig. 9. (color online) (a) Grey levels of the streak images of the signal light beam with 10 ps time interval. (b) The streak images of the signal light beam acquired by CCD with different time delay between pump and signal pulse.

Here, we omit the time jitter of laser pulses, for the achieved temporal resolution of 10 ps is much larger than the jitter of femtosecond scale. Theoretical temporal resolution of the deflector can be calculated to be 4.2 ps with $\Delta n = 0.016$. With $T = 57$ ps, the theoretical result about the number of the resolvable spots of the deflector $M = 13.6$. However, the achieved experimental temporal resolution is 10 ps. In other words, we can only distinguish five signal light streaks and $M \approx 5$ in the experiment. In addition to the reasons discussed in Section 2.2, the temporal resolution depends on many other factors such as the quality of the waveguide, the quality of the smoothness of two end faces of the deflector, non-uniform spatial distribution of pump intensity, the beginning synchronization error between the signal pulse and pump pulse, the imperfect prism array, and so on.

4. Conclusion

We have demonstrated an ultrafast beam deflection system with picosecond, even to sub-picosecond, temporal resolution, a large number of the resolvable spots, high response and repetition speed. The theoretical investigations show that material dispersion of GaAs including group velocity dispersion and angular dispersion, interface reflection, and interface scattering of the deflector, impose harmful influences on the temporal and spatial resolvable performances. Thus by properly designing the structural parameters of the deflector, a sub-picosecond scale of temporal resolution can be achieved. The experimental results show that the temporal resolution is about 10 ps, which is not very satisfying but can be improved a lot as the theoretical discussion section has suggested. In fact, we can choose proper semiconductor materials of waveguide deflector depending on the wavelength of the signal light to be deflected. For example, AlGaAs/GaAs is the proper choice for the near infrared signal light with wavelength larger than 870 nm, whose photon energy does not fall into the absorption range of the waveguide core. In the same way, the use of a wider bandgap semiconductor for the waveguide core would enable operation well into the visible spectrum, such as $Al_mGa_{1-m}As$ with a proper value of m. If $m = 0.37$ and then $\lambda_g = 650$ nm, the signal light wavelength can be larger than 650 nm. Except for the all-optical solid-state streak camera, this configuration can also be used in the optical communication, light controlling and switching, and so on.

Acknowledgment

We are very grateful to Prof. Jianlin Zhao, Dr. Xuetao-Gan, and Dr. Yadong Wang at Northwestern Polytechnical University for their contributions to this research and to Prof. Guanghua Cheng for several suggestive discussions about the experiment.

References

[1] Gordon E I 1966 *Appl. Opt.* **5** 1629
[2] Lotspeich J F 1968 *IEEE Spectrum* **5** 45
[3] Ninomiya Y 1973 *IEEE J. Quantum Elect.* **QE-9** 791
[4] Li Y, Chen D Y, Yang L and Alfano R R 1991 *Opt. Lett.* **16** 438
[5] Sakamoto T, Toyoda S, Ueno M and Kobayashi J 2014 *IEEE CPMT Symposium Japan*, November 4–6, 2014, Kyoto, Japan, p. 173
[6] Sun L, Kim J H, Jang C H, An D C, Lu X J, Zhou Q J, TaboadaJ M, Chen R T, Maki J J, Tang S N, Zhang H, Steier W H, Zhang C and Dalton L R 2001 *Opt. Eng.* **40** 1217
[7] Wight D R, Heaton J M, Hughes B T, Birbeck J C H and Hilton K P 1991 *Appl. Phys. Lett.* **59** 899
[8] Feng X, Hu W W and Xu A S 2005 *Appl. Opt.* **44** 5429
[9] Shintaro H, Kyoji S and Tetsuro K 2005 *Appl. Phys. Lett.* **87** 081101
[10] Yao L, Dao Y C, Lina Y and Alfano R R 1991 *Opt. Lett.* **16** 438
[11] Chong S, Hui L, Shining Z and Dentcho A G 2015 *Sci. Rep.* **5** 8835
[12] Wang D, Wu J Z and Zhang J X 2016 *Chin. Phys. B* **25** 064202
[13] Finch A, Liu Y, Niu H, Sibbett W, Sleat W E, Walker D R, Yang Q L ang Zhang H 1989 *Proc. SPIE* **1032** 622
[14] Liu R, Tian J S, Li H, Wang Q Q, Wang C, Wen W L, Lu Y, Liu H L, Cao X B, Wang J F, Xu X Y and Wang X 2014 *Acta Phys. Sin.* **63** 058501 (in Chinese)
[15] Friedman W, Jackal S, Seka W and Zimmermann J 1977 *Proc. SPIE* **97** 544
[16] Elliott R A and Shaw J B 1979 *Appl. Opt.* **18** 1025
[17] Sarantos C H and Heebner J E 2010 *Opt. Lett.* **35** 1389
[18] Lee B Y, Kobayashi T, Morimoto A and Sueta T 1992 *IEEE J. Quantum Elect.* **28** 1739
[19] Faris G W, Brinkman E A and Jeffries J B 2000 *Opt. Express* **7** 447
[20] Toyoshima M, Fidler F, Pfennigbauer M and Leeb W R 2006 *Opt. Express* **14** 4092
[21] Liang L L, Tian J S, Wang T, Li F L, Gao G L, Wang J F, Wang C, Lu Y, Xu X Y, Cao X B, Wen W L, Xin L W, Liu H L and Wang X 2014 *Acta Phys. Sin.* **63** 060702 (in Chinese)
[22] Lin W Z, Fujimoto L G, Ippen E P and Logan R A 1987 *Appl. Phys. Lett.* **50** 124
[23] Benjamin S D, Loka H S, Othonos A and Smith P W E 1996 *Appl. Phys. Lett.* **68** 2544
[24] Bennett B R, Soref R A and Alamo J A D 1990 *IEEE J. Quantum Elect.* **26** 113
[25] Benjamin S D, Othonos A and Smith P W E 1994 *Electron. Lett.* **30** 1704
[26] Hisatake S and Kobayashi T 2006 *Opt. Express* **14** 12704
[27] Li D R, Lv X H, Wu P, Luo Q M, Chen R W and Zeng S Q 2006 *Acta Phys. Sin.* **55** 4729 (in Chinese)
[28] Kadlec F, Nemec H and Kužel P 2004 *Phys. Rev. B* **70** 125205